Enhanced CO_2 outgassing in the Southern Ocean from a positive phase of the Southern Annular Mode

Nicole S. Lovenduski,[1] Nicolas Gruber,[1,2] Scott C. Doney,[3] and Ivan D. Lima[3]

Received 21 November 2006; revised 7 March 2007; accepted 12 April 2007; published 20 June 2007.

[1] We investigate the interannual variability in the flux of CO_2 between the atmosphere and the Southern Ocean on the basis of hindcast simulations with a coupled physical-biogeochemical-ecological model with particular emphasis on the role of the Southern Annular Mode (SAM). The simulations are run under either pre-industrial or historical CO_2 concentrations, permitting us to separately investigate natural, anthropogenic, and contemporary CO_2 flux variability. We find large interannual variability (± 0.19 PgC yr^{-1}) in the contemporary air-sea CO_2 flux from the Southern Ocean ($<35°S$). Forty-three percent of the contemporary air-sea CO_2 flux variance is coherent with SAM, mostly driven by variations in the flux of natural CO_2, for which SAM explains 48%. Positive phases of the SAM are associated with anomalous outgassing of natural CO_2 at a rate of 0.1 PgC yr^{-1} per standard deviation of the SAM. In contrast, we find an anomalous uptake of anthropogenic CO_2 at a rate of 0.01 PgC yr^{-1} during positive phases of the SAM. This uptake of anthropogenic CO_2 only slightly mitigates the outgassing of natural CO_2, so that a positive SAM is associated with anomalous outgassing in contemporaneous times. The primary cause of the natural CO_2 outgassing is anomalously high oceanic partial pressures of CO_2 caused by elevated dissolved inorganic carbon (*DIC*) concentrations. These anomalies in *DIC* are primarily a result of the circulation changes associated with the southward shift and strengthening of the zonal winds during positive phases of the SAM. The secular, positive trend in the SAM has led to a reduction in the rate of increase of the uptake of CO_2 by the Southern Ocean over the past 50 years.

Citation: Lovenduski, N. S., N. Gruber, S. C. Doney, and I. D. Lima (2007), Enhanced CO_2 outgassing in the Southern Ocean from a positive phase of the Southern Annular Mode, *Global Biogeochem. Cycles*, *21*, GB2026, doi:10.1029/2006GB002900.

1. Introduction

[2] Variations in the oceanic sources and sinks of atmospheric CO_2 are an important contributor to the interannual variability in the atmospheric CO_2 growth rate [*Bousquet et al.*, 2000; *Peylin et al.*, 2005]. Processes that regulate the exchange of CO_2 between the ocean and atmosphere are likely to change in a future characterized by global warming, leading to positive and negative feedbacks in the global climate system [*Sarmiento et al.*, 1998; *Joos et al.*, 1999; *Matear and Hirst*, 1999; *Plattner et al.*, 2001; *Gruber et al.*, 2004]. Studying the interannual variability in these processes over the last few decades and their impact on atmospheric CO_2 may help to determine the future evolution of atmospheric CO_2. Understanding the mechanisms leading to air-sea CO_2 flux variations is therefore a crucial, albeit not sufficient, condition to quantify the future behavior of the global carbon cycle. Model estimates of global interannual air-sea CO_2 flux variations are on the order of ± 0.50 PgC yr^{-1}, and suggest that they mostly originate from the Tropical Pacific [*LeQuéré et al.*, 2000; *McKinley et al.*, 2004]. Inversions of atmospheric CO_2 tend to agree with the model based results with regard to the magnitude of the variability in the Tropical Pacific [*McKinley et al.*, 2004; *Peylin et al.*, 2005], but tend to differ with regard to the magnitude of the extratropical variability in the air-sea CO_2 fluxes. Unfortunately, the observational coverage of measurements of the oceanic partial pressures of CO_2 is insufficient in most extratropical regions to establish the interannual variations in the air-sea CO_2 fluxes based on in situ data with very few exceptions [*Gruber et al.*, 2002; *Dore et al.*, 2003; *Brix et al.*, 2004; *Lefévre et al.*, 2004]. Although ill constrained, the contribution from extratropical regions is likely nonnegligible. In fact, a recent model study suggests that the Southern Ocean alone accounts for over 20% of the interannual CO_2 flux variability [*Wetzel et al.*, 2005].

[3] The unique physical oceanography of the Southern Ocean sets the stage for its important role in the global climate system. Atmospheric westerlies propel the strong

[1]Department of Atmospheric and Oceanic Sciences, University of California, Los Angeles, California, USA.
[2]Now at Institute of Biogeochemistry and Pollutant Dynamics, ETH Zurich, Zurich, Switzerland.
[3]Department of Marine Chemistry and Geochemistry, Woods Hole Oceanographic Institution, Woods Hole, Massachusetts, USA.

0886-6236/07/2006GB002900$12.00

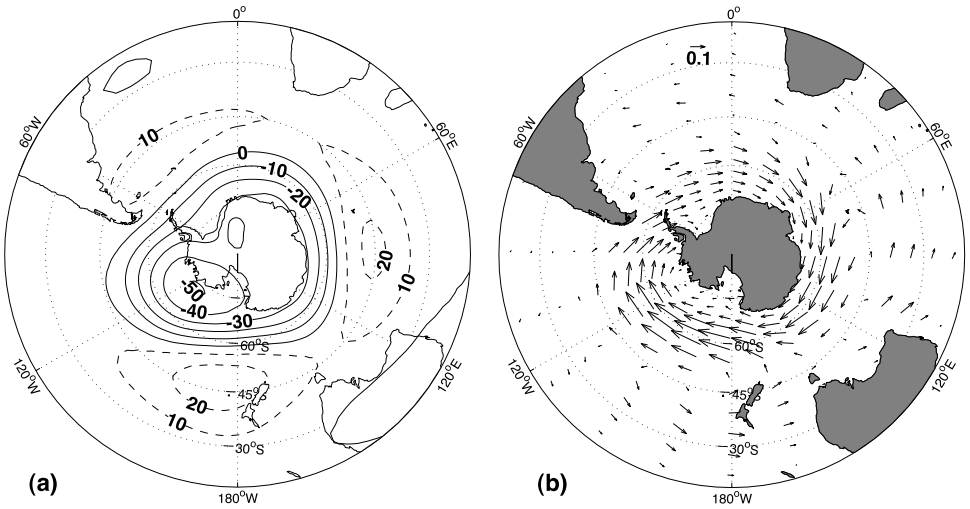

Figure 1. Regression of (a) 700 mb geopotential height anomalies (meters) and (b) wind stress anomalies (dyn cm^{-2}) onto the standardized SAM index. Regressions for the zonal and meridional components of the wind stress were calculated separately. For clarity, arrows are only drawn at every other latitude and every fifth longitude point. Note scale arrow near the top of Figure 1b.

eastward flow of the Antarctic Circumpolar Current, providing a pathway for the propagation of climatic signals from basin to basin. Westerlies also drive northward Ekman drift, creating the surface branch of a meridional overturning circulation, the Deacon Cell, that may be linked to the global thermohaline circulation [*Rintoul et al.*, 2001]. The rate of meridional overturning is critical to the processes regulating the exchange of CO_2 between the atmosphere and the Southern Ocean. Upwelling in the Antarctic Divergence exposes deep waters with elevated concentrations of dissolved inorganic carbon (*DIC*) to the surface, leading to the ventilation of natural CO_2 to the atmosphere [*Mikaloff-Fletcher et al.*, 2007; *Toggweiler and Samuels*, 1993; *Murnane et al.*, 1999]. The natural CO_2 which is lost to the atmosphere originates as respired carbon from sinking particles, and is important for determining atmospheric CO_2 on longer timescales [*Sarmiento and Toggweiler*, 1984; *Siegenthaler and Wenk*, 1984]. At the same time, approximately 40% of the global oceanic sequestration of anthropogenic CO_2 occurs on the downwelling side of the Deacon Cell [*Sabine et al.*, 2004; *Mikaloff-Fletcher et al.*, 2006], in association with the formation of mode and intermediate waters [*McCartney*, 1982]. N. Gruber et al. (Oceanic sources and sinks for atmospheric CO_2, submitted to *Global Biogeochemical Cycles*, 2007) (hereinafter referred to as Gruber et al., submitted manuscript, 2007) estimate that this high rate of uptake of anthropogenic CO_2 has turned the Southern Ocean from a preindustrial source of CO_2 to the atmosphere to a net sink for atmospheric CO_2, consistent with the new pCO_2 climatology of T. Takahashi et al. (Climatological mean and decadal change in surface ocean pCO_2, and net sea-air CO_2 flux over the global oceans, manuscript in preparation, 2007) (hereinafter referred to as Takahashi et al., manuscript in preparation, 2007). Given the large exchange fluxes of both natural and anthropogenic CO_2, and the potential for sensitivity to future climate change [*Sarmiento et al.*, 1998], it is pertinent to understand how this region responds to climate variability and how it might be affected by climate change.

[4] Both observations [*Lovenduski and Gruber*, 2005; *Hughes et al.*, 2003; *Liu et al.*, 2004] and models [*Hall and Visbeck*, 2002; *Oke and England*, 2004; *Watterson*, 2000] have shown that most of the interannual climatic variability in the Southern Ocean is closely tied to the Southern Annular Mode (SAM), the dominant mode of atmospheric interannual variability in the extratropical circulation of the Southern Hemisphere [*Thompson and Wallace*, 2000]. The spatial pattern associated with the SAM represents a nearly zonally symmetric oscillation of pressure over the Pole and pressure over midlatitudes (Figure 1a). The SAM index is defined as the leading principal component of monthly geopotential height anomalies south of 20°S, such that positive SAM is associated with anomalously low pressure over the Pole. Such a positive SAM is also coincident with a poleward shift of the westerly winds (Figure 1b) [*Hartmann and Lo*, 1998; *Limpasuvan and Hartmann*, 1999; *Lovenduski and Gruber*, 2005]. Since air-sea CO_2 flux is directly influenced by wind speed, and wind anomalies can alter the circulation and biogeochemistry of the ocean, and hence the oceanic pCO_2, it is likely that wind anomalies associated with the SAM can impact the flux of CO_2 between the atmosphere and the Southern Ocean.

[5] Here we use output from a hindcast simulation of a global ocean general circulation model with an embedded biogeochemical-ecological model to investigate the interannual variability in the flux of CO_2 between the atmosphere and the Southern Ocean under contemporary conditions. We then separately investigate how much of this variability is driven by the air-sea flux of natural carbon, and how much by the flux of anthropogenic CO_2. This separation is made by running the model using either a constant pre-industrial

atmospheric CO_2 (278 μatm) or the time-varying historical atmospheric CO_2 record over the last 250 years as surface boundary conditions. The difference between these two runs is considered anthropogenic CO_2, while the fluxes in the pre-industrial simulation are just that of natural carbon. Defined this way, the only factor driving the oceanic uptake of anthropogenic CO_2 is the anthropogenic perturbation of atmospheric CO_2. The anthropogenic CO_2 uptake rate is then modified by variability and trends in ocean circulation, wind speed, and the surface ocean buffer factor [*Gruber et al.*, 2004]. In contrast, the air-sea exchange flux of natural carbon is not impacted by changes in atmospheric CO_2, but responds to all climate variability induced changes of the relevant driving factors, such as wind speed, temperature, salinity, ocean circulation, and ocean biology. Trends in the physical forcing, whether of anthropogenic origin or not, will impact both anthropogenic and natural CO_2 fluxes. However, as we will see, it is primarily the natural CO_2 fluxes that are responding to climate variability and change. Additionally, we quantify the relationship between anomalies in the air-sea flux of contemporary, natural, and anthropogenic CO_2 and the SAM and analyze the mechanisms responsible for CO_2 flux variability associated with the SAM.

[6] Using similar approaches, but employing different ocean circulation and biogeochemical models, two recent studies have also begun to explore the relationship between the SAM and Southern Ocean CO_2 fluxes. *Lenton and Matear* [2007] used the ocean component of the CSIRO model with similar forcing, but undertook just a historical simulation. As a result, they were only able to investigate the variability of the contemporary air-sea CO_2 flux, while our running of both historical and pre-industrial simulations permits us to separately determine the impact of the SAM on natural and anthropogenic CO_2 fluxes. *Wetzel et al.* [2005] also explored air-sea CO_2 flux variability in the Southern Ocean and its connection to SAM. Similar to Lenton and Matear, they found anomalous outgassing of CO_2 during positive phases of the SAM. *Wetzel et al.* [2005] also noted an outgassing trend in the air-sea CO_2 flux from the Southern Ocean, and suggested that the trend was likely related to a trend in the SAM. This positive trend in the SAM over the past few decades [*Thompson et al.*, 2000; *Thompson and Solomon*, 2002] may itself be linked to climate change at high latitudes [*Carril et al.*, 2005]. Here we extend on these two studies with a more in-depth analysis, and use a more realistic ecosystem model coupled to an advanced global ocean general circulation model. We confirm the basic findings of these prior studies in that positive SAM leads to an anomalous outgassing, but demonstrate also the importance of the differential impact of SAM on natural and anthropogenic CO_2. We also elucidate that the main driver for the changes are alterations in the meridional overturning circulation, as suggested by *Lovenduski and Gruber* [2005].

2. Methods

[7] We determine the interannual variability of the air-sea CO_2 fluxes in the Southern Ocean on the basis of hindcast simulations using a state-of-the-art biogeochemical-ecological model that has been coupled to the Parallel Ocean Program (POP) ocean general circulation model. POP is a level-coordinate, hydrostatic, primitive equation model integrated here with a resolution of 3.6° in longitude, 0.8° to 1.8° in latitude, and 25 vertical levels [*Yeager et al.*, 2006]. The effects of eddy transport are parameterized according to *Gent and McWilliams* [1990]. The biogeochemical-ecological model is taken from the NCAR global Community Climate System Model (CCSM) and consists of a multiple phytoplankton functional group model for the euphotic zone processes, and a relatively simple biogeochemical model for the aphotic zone processes. This model comprises several nutrient, phytoplankton, zooplankton, and detritus components, and contains complex ecosystem parameterizations, including an iron cycle. The model equations are identical to those reported for the 3-D implementation of *Moore et al.* [2004] with two important modifications as documented in more detail by *Moore et al.* [2006]. First, water column denitrification has been added to the model in order to close the global nitrogen cycle. Second, a number of the parameters associated with the model iron dynamics and scavenging have been adjusted to improve the simulated dissolved iron fields [see *Moore et al.*, 2006, Table 1].

[8] The coupled physical-biogeochemical-ecological model is first spun up to an approximate cyclostationary state with prescribed repeating annual cycles of physical forcing and dust deposition and a pre-industrial atmospheric CO_2 mixing ratio of 278 ppm. Two separate hindcast simulations are then performed with the model. In the first, atmospheric CO_2 is held at a constant pre-industrial value of 278 ppm, and in the second, the model is run using the measured and reconstructed evolution of atmospheric CO_2 from 1765 to 2004 as a boundary condition. We refer to the former as the pre-industrial simulation and the latter as the historical simulation. The CO_2 fluxes from the pre-industrial simulation are driven by the cycling of natural CO_2, while the CO_2 fluxes from the historical run represent the sum of natural and anthropogenic CO_2. We determine the flux of anthropogenic CO_2 by subtracting the CO_2 flux in the pre-industrial simulation from the CO_2 flux in the historical simulation. In doing so, we assume that variations in the natural carbon cycle have no influence on the uptake of anthropogenic CO_2. This assumption is not without caveats, as variations in the natural carbon cycle change the buffer (Revelle) factor of the ocean [*Sarmiento and Gruber*, 2006, chap. 8], and hence can alter the ocean's capacity for taking up anthropogenic CO_2 from the atmosphere. However, since model simulations that include/exclude an active natural carbon cycle give very similar results with regard to the uptake of anthropogenic CO_2 [*Watson and Orr*, 2003], we judge the impact of the interaction between the natural and anthropogenic carbon cycle to be small. Both the historical and pre-industrial simulations are brought from the initial cyclo-stationary state (1765) to 1957 using repeating annual cycles of physical forcing following *Doney et al.* [2007]. Then, both simulations are forced with 6-hourly heat, monthly freshwater, and 6-hourly momentum fluxes computed using bulk transfer formula and surface atmosphere data from the National Center for Environmental

Table 1. Annual Mean Air-Sea Fluxes of Modeled Contemporary, Natural, and Anthropogenic CO_2 (Pg C yr^{-1})[a]

		Contemporary			Natural		Anthropogenic	
Region	Latitudes	Model[b,c]	Inversion	Observed[d]	Model[b]	Inversion	Model[c]	Inversion
South Atlantic, low latitude	18°S–31°S	0.04	−0.01 ± 0.01	0.03	0.08	0.02 ± 0.01	−0.03	−0.02 ± 0.01
South Atlantic, midlatitude	31°S–44°S	−0.34	−0.16 ± 0.05	−0.16	−0.26	−0.11 ± 0.05	−0.07	−0.05 ± 0.02
South subpolar Atlantic	44°S–58°S	−0.05	0.00 ± 0.08	−0.13	−0.02	0.11 ± 0.05	−0.08	−0.11 ± 0.07
Southern Ocean	S. of 58°S	0.08	−0.20 ± 0.11	0.01	0.25	0.04 ± 0.04	−0.19	−0.24 ± 0.10
Southwest Pacific, midlatitude	18°S–44°S	−0.58	−0.44 ± 0.10	−0.36	−0.46	−0.35 ± 0.09	−0.13	−0.09 ± 0.04
Southeast Pacific, midlatitude	18°S–44°S	0.09	−0.02 ± 0.03	0.04	0.15	−0.01 ± 0.03	−0.04	−0.02 ± 0.01
South subpolar Pacific and Ind	44°S–58°S	0.10	−0.14 ± 0.15	−0.31	0.27	0.25 ± 0.09	−0.23	−0.39 ± 0.12
Southern Indian, midlatitude	18°S–44°S	−0.52	−0.46 ± 0.09	−0.46	−0.38	−0.22 ± 0.06	−0.16	−0.24 ± 0.07
Sum of Regions		−1.18	−1.43 ± 0.25	−1.34	−0.37	−0.27 ± 0.17	−0.93	−1.16 ± 0.19

[a]Flux estimates from ocean inversions and observations are shown for comparison. Positive values indicate ocean outgassing. Inversion estimates are taken from [*Mikaloff-Fletcher et al.*, 2006, 2007], while observational estimates are from Takahashi et al. (manuscript in preparation, 2007).
[b]Regional estimates have been adjusted for a global −0.52 Pg C yr^{-1} drift, scaled by area.
[c]Model estimates of contemporary and anthropogenic fluxes represent an average from 1990 to 2000.
[d]Fluxes computed on the basis of the ΔpCO_2 values reported by Takahashi et al. (manuscript in preparation, 2007) using the *Wanninkhof* [1992] formulation for the gas transfer velocity.

Prediction/National Center for Atmospheric Research (NCEP/NCAR) reanalysis [*Kalnay et al.*, 1996], as well as satellite data products including daily Goddard Institute for Space Studies radiation and Special Sensor Microwave/Imager monthly ice fraction from 1958 through 2004 [*Large and Yeager*, 2004]. There is a repeating annual cycle of surface dust flux [*Mahowald et al.*, 2003] in both simulations. Gas exchange is parameterized using a quadratic wind speed relationship as described by *Wanninkhof* [1992].

[9] After analyzing the modeled mean state, we conduct statistical analyses on monthly anomalies of model output from 1958 through 2004. Monthly anomalies represent what remains after the climatological mean seasonal cycle and linear trend have been removed from the output at each location and depth. Seasonal cycles were calculated by binning all output into 12 monthly bins and then taking the average. Linear trends were removed from all of the preindustrial output, as well as most of the historical output. The trends removed from historical air-sea CO_2 fluxes, surface ocean pCO_2, and *DIC* were determined by finding the least squares fit to the data as a linear function of the historical atmospheric CO_2 curve. With the exception of Table 1, we ignore the modeled drift in air-sea CO_2 flux. We correlate and regress anomalies onto a standardized SAM index, using the method of *Bretherton et al.* [1999] to determine the statistical significance of correlation coefficients in the presence of autocorrelation.

[10] Statistical analyses are performed on both a point-by-point and regional average basis. In the case of the regional averages, the Southern Ocean is divided into four distinct zones, whose boundaries are well-known fronts. These fronts represent steep gradients in vertical structure, temperature, salinity, and nutrient concentration. The fronts we use here were derived from satellite sea surface temperature (SST) data [*Moore et al.*, 1999], as well as data collected during meridional section cruises [*Belkin and Gordon*, 1996]. It is unlikely that this will lead to artifacts in the analysis, as the position of the observed fronts nearly corresponds to those derived from the model (not shown). For the purposes of our analysis, we assume the fronts are stationary. The Antarctic Zone (AZ) is defined as the region south of the Antarctic Polar Front (APF) [*Moore et al.*, 1999]. The Polar Frontal Zone (PFZ) is the region between the APF and the Subantarctic Front (SAF), and the Subantarctic Zone (SAZ) is the region between the SAF and the South Subtropical Front (SSTF). The Subtropical Zone (STZ) is bordered by the SSTF and the North Subtropical Front (NSTF) [*Belkin and Gordon*, 1996]. Anomaly time series of output from each region are created by averaging the anomalies of all points within the region.

[11] The SAM index used here is the first principal component of the monthly 700 mb geopotential height anomalies south of 20°S from 1958–2004 obtained from the NCEP/NCAR reanalysis (Figure 1a). The index is standardized by subtraction of the mean and division by the standard deviation. Since it is believed that the SAM has a relatively weak seasonality [*Hall and Visbeck*, 2002; *Hartmann and Lo*, 1998], we use year-round data to construct the index. Our index correlates with the monthly SAM index from the NOAA Climate Prediction Center (1979–2004) [http://www.cpc.ncep.noaa.gov] at r = 0.97.

3. Model Evaluation

[12] The successful modeling of the interannual and long-term variations in the air-sea CO_2 fluxes requires a well evaluated model, whose strengths and weaknesses are well established. Owing to the sparseness of carbon related observations in the Southern Ocean, and the importance of ocean physics in determining our results, we limit the evaluation to the interannual variations of a few physical parameters (SST, sea-surface height), and the annual mean air-sea CO_2 fluxes from ocean inversion models and surface pCO_2 observations.

[13] The SST in the physical model and in the real ocean respond in a similar way to anomalous surface forcing associated with the SAM. To compare the two, we use satellite observations of monthly averaged SST from AVHRR Oceans Pathfinder (versions 4.1 and interim 4.1) on a 9 km grid from 1985–2003 (http://podaac.jpl.nasa.gov). Anomalies in SST were interpolated to a 1° grid, and surface temperature anomaly time series from the model

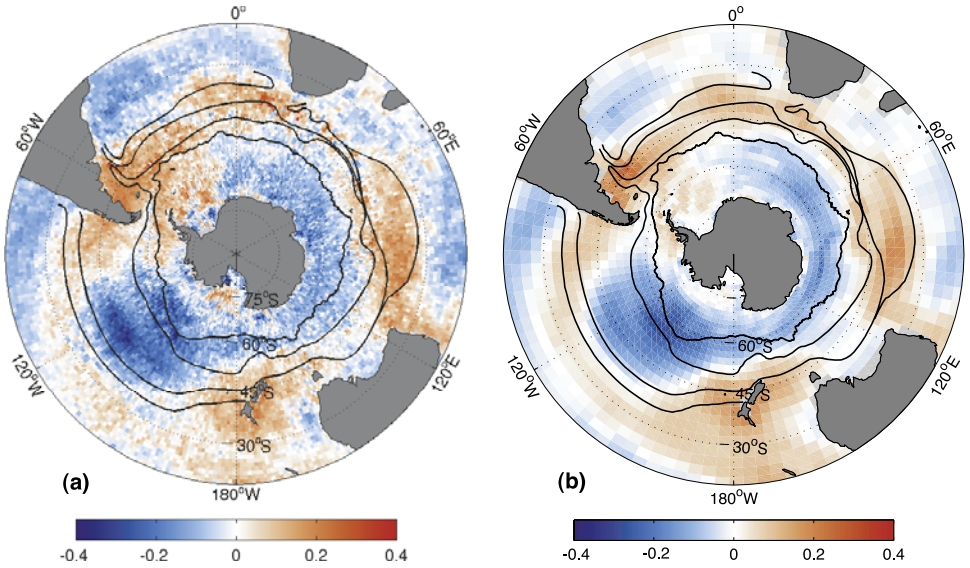

Figure 2. Regression of (a) observed SST anomalies and (b) model SST anomalies from the historical simulation onto the standardized SAM index (°C). Black contours mark the location of the Southern Ocean fronts. From pole to equator these fronts are: APF, SAF, SSTF, and NSTF.

were sampled to match the months of available SST data. Figure 2 shows the regression of the observed and modeled surface temperature anomalies onto the SAM index. The two regression patterns are nearly identical, indicating that the modeled SST response to the SAM compares well with the observed response. To illustrate this point further, we calculated the regression coefficients of the regional anomaly time series in both observed and modeled surface temperature with the SAM (not shown). The regression coefficients are indistinguishable in the AZ and PFZ, but there are small biases in the model regressions in the SAZ and STZ. One possible cause for this offset is that while the observations represent the skin temperature of the ocean, temperature in the first layer of the model represents an average over the top 8 m. Another possible model bias is the lack of explicit consideration for the role of eddies, which are particularly abundant in the SAZ and STZ.

[14] Similar success is found in the model's ability to simulate ship-based heat content and ship and satellite-based sea-surface height variability [see *Doney et al.*, 2007], although they describe results from an earlier version of the POP model.

[15] The coupled ocean physical-biogeochemical-ecological model reproduces quite successfully the annual mean air-sea CO_2 flux patterns in the Southern Ocean, as estimated by ocean inversion models and observations. Figure 3 shows the annual mean contemporary (1990–2000), natural (1958–2000), and anthropogenic (1990–2000) air-sea CO_2 fluxes from the model, with positive fluxes into the atmosphere. The contemporary and natural CO_2 fluxes are that of outgassing in the region south of ~55°S, while the mode water formation regions between ~40–55°S are regions of contemporary and natural CO_2 uptake. Anthropogenic CO_2 is everywhere being taken up by the Southern Ocean in the annual mean, with most of the uptake occurring in the upwelling regions of the AZ and the mode water formation regions in the Atlantic and Indian basins. These patterns of contemporary, natural, and anthropogenic uptake and outgassing agree with inverse model estimates from *Mikaloff-Fletcher et al.* [2006, 2007] and with observed estimates from Takahashi et al. (manuscript in preparation, 2007) in the Southern Ocean regions used for this study (Table 1). While flux estimates may differ in the individual regions, the fluxes integrated over the entire Southern Ocean agree to within the uncertainties. Global estimates of air-sea CO_2 flux from this model are also well matched with inversion estimates and observations (not shown), particularly in terms of anthropogenic CO_2, whose annual mean modeled global uptake (1990–2000) is 1.98 PgC yr^{-1}, in agreement with a large range of independent estimates (as summarized by Gruber et al. (submitted manuscript, 2007)).

[16] From these comparisons, we conclude that the coupled model demonstrates reasonable skill in its representation of the mean state and how this mean state is perturbed by interannual variations in surface forcing. This gives us some confidence in the modeled air-sea CO_2 flux variability, discussed next.

4. Variability of Air-Sea CO_2 Fluxes

[17] The time series of the Southern Ocean (<35°S) integrated air-sea CO_2 fluxes in Figure 4 reveal a positive trend (less oceanic uptake with time) for natural CO_2, while the flux of anthropogenic CO_2 shows a strong negative trend (more oceanic uptake with time). The latter is expected as it reflects the oceanic response to increased atmospheric CO_2 concentration in the historical run, while it has been proposed that the former is due to a trend in the SAM index [*Wetzel et al.*, 2005], as discussed in more detail below. The anthropogenic CO_2 trend exceeds that for natural CO_2, so that the contemporary air-sea flux also

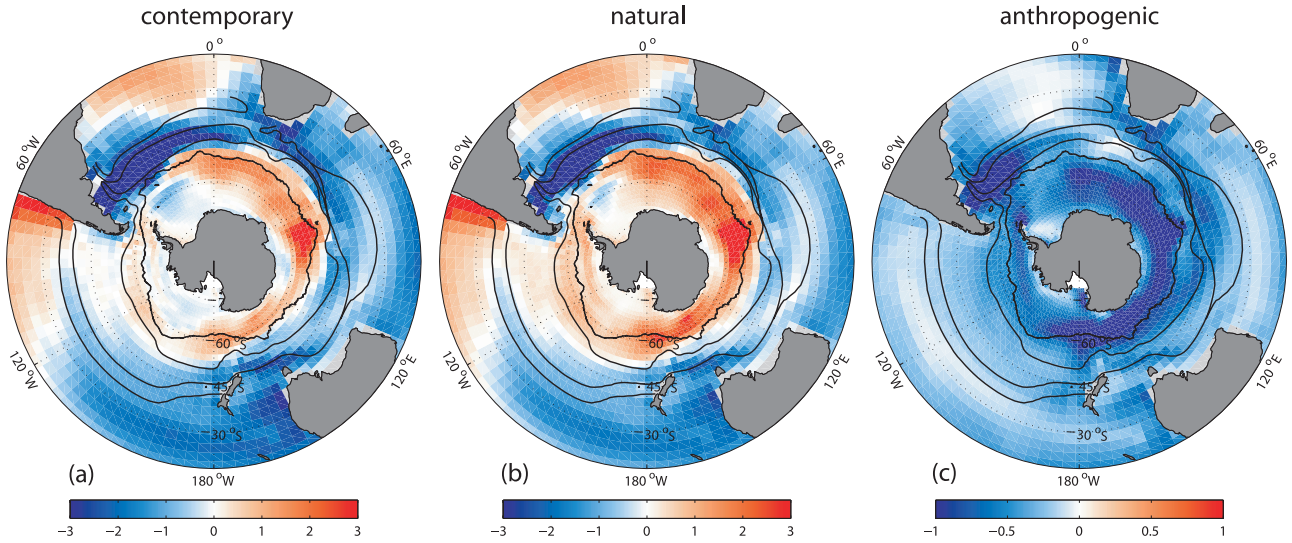

Figure 3. Annual mean air-sea flux of (a) contemporary CO_2 (natural + anthropogenic CO_2), (b) natural CO_2, and (c) anthropogenic CO_2 (mol m^{-2} yr^{-1}). The fluxes have been averaged using output from the historical simulation for Figure 3a, preindustrial simulation for Figure 3b, and from their difference for Figure 3c. Positive fluxes indicate ocean outgassing. Note difference in scale for the anthropogenic flux.

exhibits a negative trend. With regard to variations around these trends, Figure 4 suggests that most of the contemporary flux variability originates from variability in natural rather than anthropogenic CO_2. We first investigate the variability by focusing our analysis on model output that has been both deseasonalized and detrended, and return to the trends at the end.

[18] The contemporary and natural air-sea CO_2 flux anomalies shown in Figure 5 exhibit large variability for the Southern Ocean: ±0.19 PgC yr^{-1} and ±0.18 PgC yr^{-1}, respectively (1σ). These flux variances are substantially larger than those obtained previously for the Southern Ocean from ocean model simulations (e.g., ±0.1 PgC yr^{-1} from *Peylin et al.* [2005] and ±0.05 PgC yr^{-1} from *Wetzel et al.* [2005]). The model simulated contemporary and natural CO_2 flux variability from the Southern Ocean accounts for 30% of the global variance in these fluxes, which is in line with the estimated contribution from the Southern Ocean in other models [*Wetzel et al.*, 2005; *LeQuéré et al.*, 2000]. The contemporary and natural monthly time series are well correlated (r = 0.96), and exhibit similar spatial patterns of variance (Figure 6). In contrast, interannual variability in the air-sea flux of anthropogenic CO_2 does not exhibit high correlations with either contemporary or natural flux anomalies and is considerably smaller(±0.05 Pg C yr^{-1} (1σ), Figure 6). As atmospheric CO_2 concentrations grow throughout the simulation, variability in the anomalous anthropogenic CO_2 fluxes increases slightly.

[19] Variance in the CO_2 flux anomalies is elevated in the region south of ~45°S (Figure 6), where the SAM is likely to have an influence on air-sea flux variability. Indeed, there is a clear connection between both the contemporary and

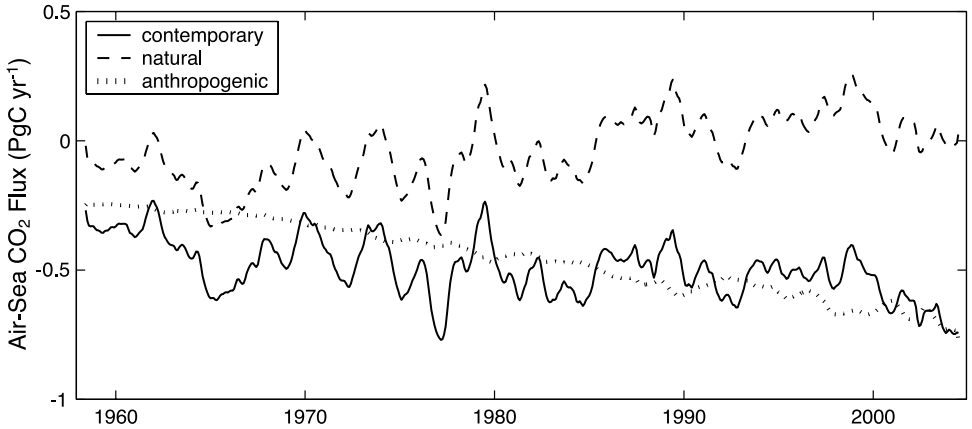

Figure 4. Mean Southern Ocean (<35°S) air-sea CO_2 flux, smoothed with an 12-month running average (PgC yr^{-1}). Negative fluxes indicate ocean uptake.

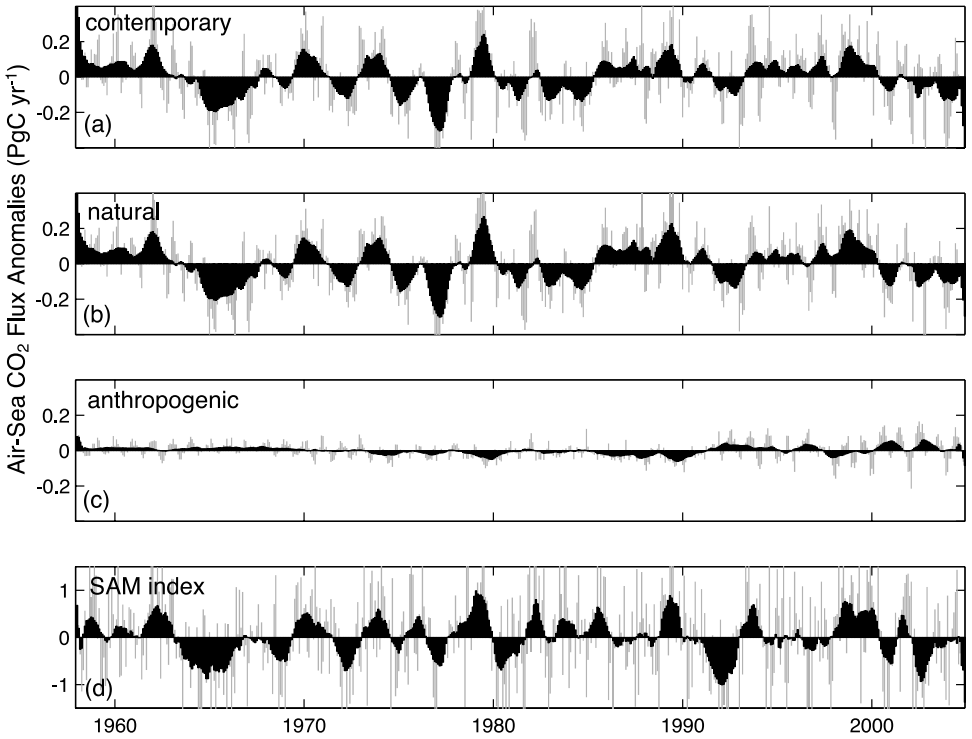

Figure 5. Southern Ocean air-sea flux anomalies of (a) contemporary, (b) natural, and (c) anthropogenic CO_2 (PgC yr^{-1}). (d) Standardized SAM index used in this study. Each time series has been smoothed with a 12-month running average, with the monthly time series displayed behind in gray. Positive fluxes indicate ocean outgassing.

natural air-sea CO_2 flux variability in the Southern Ocean (<35°S) and the SAM (Figure 5). The SAM explains 21% and 31% (r^2) of the variance in the contemporary and natural CO_2 flux anomalies, respectively (Table 2). When the time series are filtered with a 12-month running mean, the SAM explains 43% (r^2) of the variance in the contemporary CO_2 flux anomalies and 48% of that for natural CO_2 (Table 2). This implies that their relationship is stronger at lower frequencies. When the SAM leads the contemporary and natural CO_2 flux anomalies by one month (lag 1), the

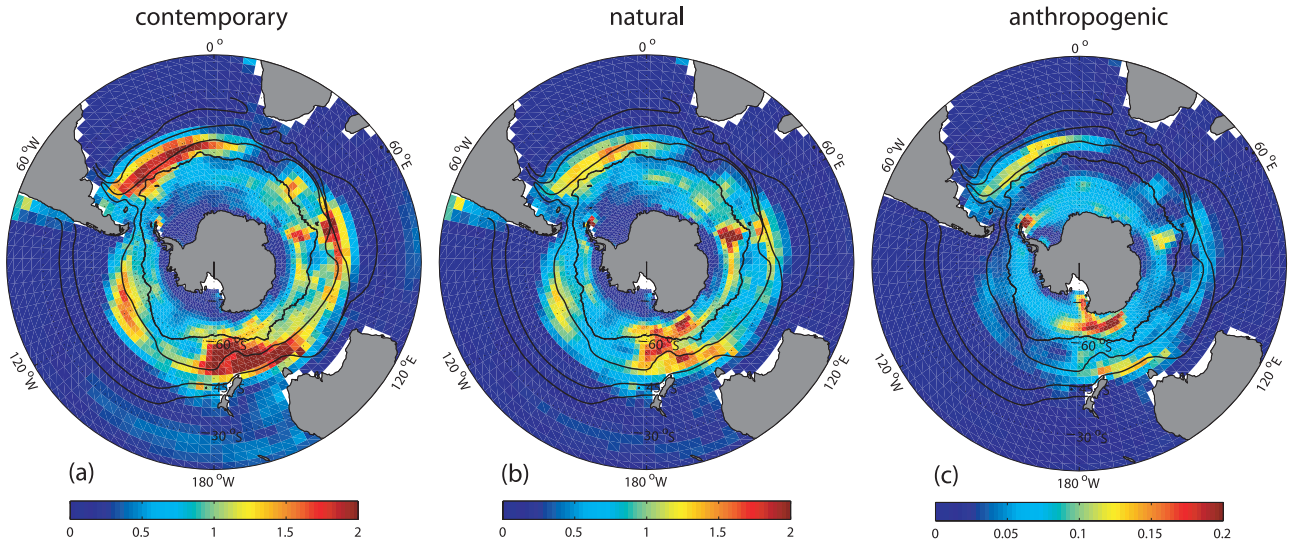

Figure 6. Variance of air-sea flux anomalies of (a) contemporary, (b) natural, and (c) anthropogenic CO_2 (mol m^{-2} yr^{-1})^2. Note that the scale of Figure 6c is 10 times smaller than that used in Figures 6a and 6b.

Table 2. Relationship Between Spatially Integrated (<35°S) Air-Sea CO_2 Flux Anomalies and the Standardized SAM Index

Quantity	Contemporary	Natural	Anthropogenic
	Regressions, *PgC yr*$^{-1}$		
Regression with SAM	0.09	0.10	−0.01
Smoothed regression[a]	0.16	0.18	−0.02
Lag-1 Regression[b]	0.08	0.08	0
	Correlations (*r*)		
Correlation with SAM	0.46	0.56	−0.28
Smoothed correlation[a]	0.66	0.69	−0.35
Lag-1 correlation[b]	0.42	0.47	−0.09

[a]A 12-month running average was used.
[b]The SAM leads the CO_2 fluxes by 1 month, without smoothing.

correlation with the SAM remains high (Table 2), suggesting that any anomalous contemporary or natural CO_2 flux linked to the SAM can persist for at least one month. In the rest of this paper, however, we focus only on the monthly relationship at zero lag. Anthropogenic CO_2 flux anomalies have a weaker relationship with the SAM when spatially integrated over the Southern Ocean (Table 2), although we will see next that climate variations associated with the SAM can slightly change the rate of anthropogenic CO_2 uptake.

[20] Positive phases of the SAM are associated with significant anomalous outgassing of both contemporary and natural CO_2 throughout a large fraction of the Southern Ocean, as revealed by Figure 7. When integrated over the region south of 35°S, the rates of anomalous outgassing during a $+1\sigma$ SAM are 0.09 and 0.10 PgC yr^{-1} for contemporary and natural CO_2, respectively (Table 2). In contrast, positive phases of the SAM are associated with small, but significant uptake of anthropogenic CO_2 in the same region, where the rate of anomalous uptake during a $+1\sigma$ SAM is 0.01 PgC yr^{-1} (Table 2). Anomalies in the outgassing and uptake stand out most clearly in the region south of 55°S, where the regression coefficients are nearly zonally symmetric. However, regionally averaged time series of contemporary, natural, and anthropogenic CO_2 flux anomalies have strong relationships with the SAM in all four regions of the Southern Ocean, as demonstrated in Figure 8. Contemporary CO_2 outgassing is enhanced by 28% in the AZ and 33% in the PFZ during positive SAM, where enhanced outgassing of natural CO_2 is only slightly mitigated by enhanced uptake of anthropogenic CO_2. In the SAZ and STZ, positive phases of the SAM are associated with a reduction of contemporary CO_2 uptake. This reduction is mostly driven by the natural CO_2 response, as the anthropogenic response is small and only significant in the STZ (Figure 8). We find a larger anomalous anthropogenic

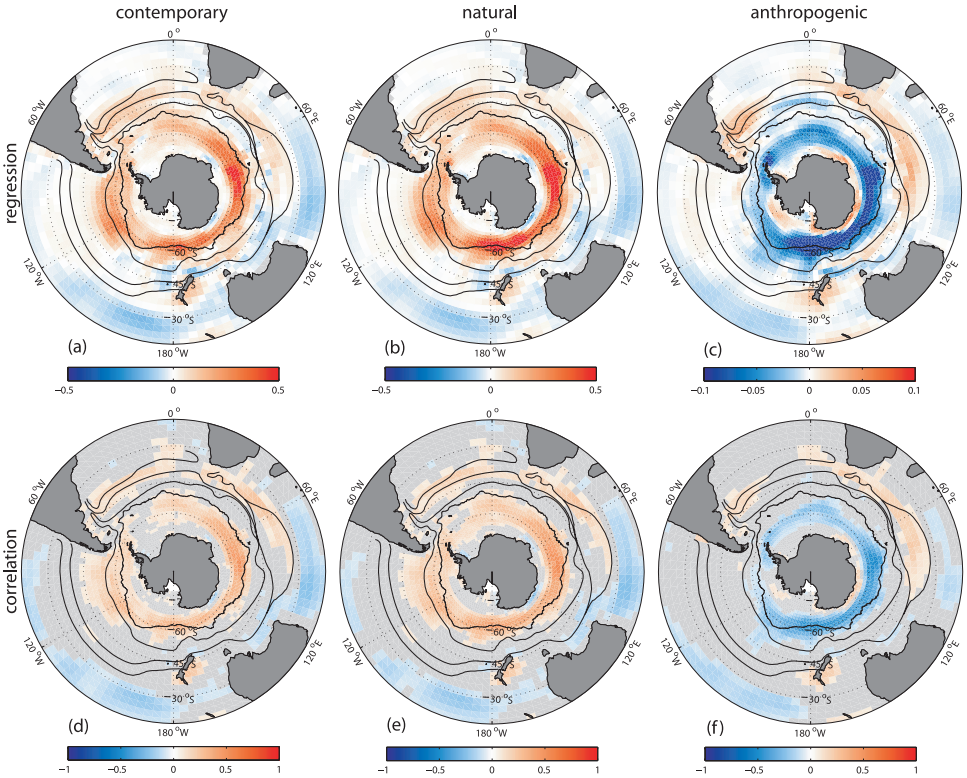

Figure 7. (a–c) Regression (mol m^{-2} yr^{-1}) and (d–f) correlation of (Figures 7a and 7d) contemporary, (Figures 7b and 7e) natural, and (Figures 7c and 7f) anthropogenic air-sea CO_2 flux anomalies with the SAM index. Regression coefficients correspond to 1 standard deviation change in the SAM index. Only those correlation coefficients with significance ≥95% are shown. Positive fluxes indicate ocean outgassing. Note that the scale of Figure 7c is 20% of Figures 7a and 7b.

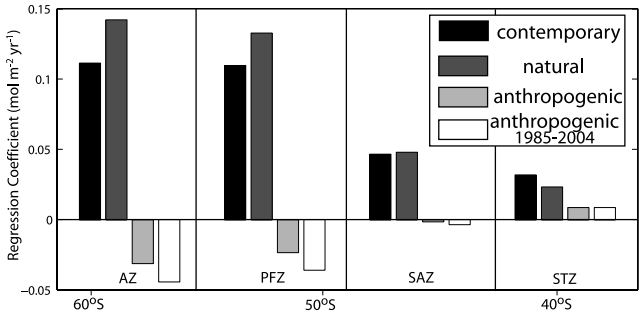

Figure 8. Regression coefficient of the SAM index with the regionally averaged time series of the air-sea flux anomalies of contemporary, natural, and anthropogenic air-sea CO_2 (mol m^{-2} yr^{-1}). Regression coefficients of anthropogenic CO_2 flux anomalies from the last 20 years (1985–2004) with the SAM are also plotted. Regression coefficients correspond to 1 standard deviation change in the SAM index. All regressions are statistically significant at >95%, with the exception of the anthropogenic coefficients in the SAZ.

CO_2 uptake in the AZ and PFZ during positive SAM over the last 20 years of the simulation (Figure 8), suggesting that the mitigating role of this component could become more important in the future.

5. Causes of the Variability

[21] In order to ascertain the mechanisms governing the contemporary CO_2 flux anomalies during positive SAM, it is most insightful to investigate the flux anomalies of natural and anthropogenic CO_2 separately. We focus first on the natural CO_2 flux anomalies by performing postprocessing calculations on monthly output, and then briefly study the anthropogenic CO_2 flux anomalies.

[22] We investigate the mechanisms responsible for the anomalous natural air-sea CO_2 flux during positive SAM by considering the total derivative of the air-sea CO_2 flux. As the model uses a standard bulk parameterization for the computation of this flux, the parameters to be considered are the gas exchange coefficient (modeled as a function of wind speed (*WS*), temperature (*T*), and salinity (*S*)), the sea ice fraction (*Ice*), and surface ocean pCO_2 (pCO_2^{oc}). Here we can neglect variations in atmospheric pressure and pCO_2 as it is assumed constant in the preindustrial simulation. Furthermore, variations in temperature and salinity have a relatively small impact on the gas exchange coefficient, so that we consider only the impact of wind speed. This yields for the relative contribution of each parameter to the anomalous air-sea CO_2 flux in each Southern Ocean region, ΔF,

$$\Delta F = \frac{\partial F}{\partial WS}\Delta WS + \frac{\partial F}{\partial Ice}\Delta Ice + \frac{\partial F}{\partial pCO_2^{oc}}\Delta pCO_2^{oc}, \qquad (1)$$

where $\frac{\partial F}{\partial WS}$, $\frac{\partial F}{\partial Ice}$, and $\frac{\partial F}{\partial pCO_2^{oc}}$ are determined from the model equations and mean values in each region. ΔWS and ΔIce are the differences of the mean wind speed and ice fraction, respectively, during a one standard deviation positive phase of the SAM and their mean values. The contribution to ΔpCO_2^{oc} is further decomposed into contributions from *DIC*, alkalinity (*Alk*), temperature, and salinity,

$$\Delta pCO_2^{oc} = \frac{\partial pCO_2^{oc}}{\partial DIC}\Delta DIC + \frac{\partial pCO_2^{oc}}{\partial Alk}\Delta Alk + \frac{\partial pCO_2^{oc}}{\partial T}\Delta T + \frac{\partial pCO_2^{oc}}{\partial S}\Delta S. \qquad (2)$$

[23] As changes in *DIC* and *Alk* and hence changes in pCO_2 can be driven by variations in freshwater fluxes (Δfw) [see, e.g., *Keeling et al.*, 2004] as well as by variations in ocean internal biogeochemical processes and transport/mixing, it is useful to separate the two mechanisms. We achieve this by expanding the total derivatives and introducing salinity-normalized *DIC* (*sDIC*) and salinity normalized *Alk* (*sAlk*) (see Appendix A for more details). Substituting (2) and (A1)–(A3) into (1) yields

$$\Delta F = \frac{\partial F}{\partial WS}\Delta WS + \frac{\partial F}{\partial Ice}\Delta Ice + \frac{S}{S_0}\frac{\partial F}{\partial DIC}\Delta sDIC + \frac{S}{S_0}\frac{\partial F}{\partial Alk}\Delta sAlk + \frac{\partial F}{\partial fw}\Delta fw + \frac{\partial F}{\partial T}\Delta T + \frac{\partial F}{\partial S}\Delta S, \qquad (3)$$

whose individual terms are shown in Table 3 and Figure 9a.

[24] The analysis of the total derivative of the air-sea flux of natural CO_2 during a positive phase of SAM (Table 3, Figure 9a) demonstrates that variations in *sDIC* and/or wind speed tend to dominate the overall response, and that their contribution is generally countered by opposing tendencies arising from temperature variations [*Doney et al.*, 2006]. The contribution of the other terms, such as *sAlk*, sea-ice, *fw*, and salinity is comparatively small. Wind speed tends to dominate in the Antarctic Zone (AZ) and the Subtropical Zone (STZ). The flux in the AZ is especially sensitive to wind speed changes, and the AZ experiences a large anomaly in wind speed during positive SAM. In the STZ, however, $\frac{\partial F}{\partial WS}$ is negative, so that a decrease in wind speed

Table 3. Estimated Contributions to the Air-Sea CO_2 Flux Anomalies, ΔF, as in Equation (3)[a]

Quantity	AZ	PFZ	SAZ	STZ
	Individual Terms			
$\frac{\partial F}{\partial WS}\Delta WS$	0.28	0.07	−0.03	0.11
$\frac{\partial F}{\partial Ice}\Delta Ice$	−0.03	0	0	0
$\frac{S}{S_0}\frac{\partial F}{\partial DIC}\Delta sDIC$	0.21	0.40	0.23	0.01
$\frac{S}{S_0}\frac{\partial F}{\partial Alk}\Delta sAlk$	0.04	0.05	0.02	0.01
$\frac{\partial F}{\partial fw}\Delta fw$	0.02	0.01	0	0
$\frac{\partial F}{\partial T}\Delta T$	−0.09	−0.24	−0.15	−0.07
$\frac{\partial F}{\partial S}\Delta S$	0.01	0.01	0	0
	Sum of Terms Versus Modeled			
Σ	0.44	0.30	0.07	0.06
ΔF_{mod}	0.25	0.21	0.09	−0.03

[a]Units are mol m^{-2} yr^{-1}. Positive fluxes are to the atmosphere. Σ is the sum of all seven terms, and ΔF_{mod} is the modeled anomaly in *F* during positive SAM.

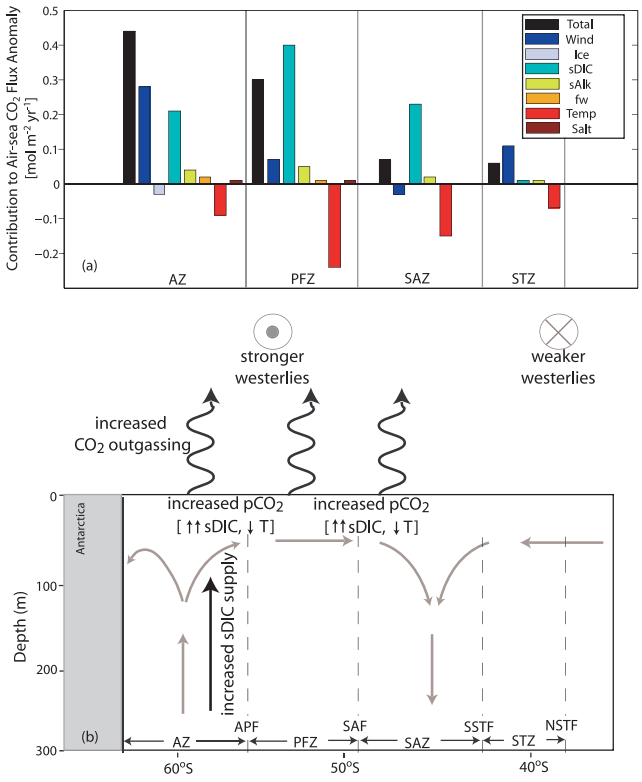

Figure 9. (a) Contribution to the air-sea CO_2 flux anomaly, ΔF, as in equation (4) (mol m^{-2} yr^{-1}). (b) Schematic illustration of the upper ocean response to a positive phase of the SAM in the pre-industrial simulation.

during positive SAM leads to anomalous outgassing. The contribution from *sDIC* dominates in the Polar Frontal Zone (PFZ) and the Subantarctic Zone (SAZ), and plays a secondary role in the AZ. During positive SAM, we find increased *sDIC* in the AZ, PFZ, and SAZ (Figure 10a, Table 4), leading to considerable $\Delta sDIC$ values in these regions. Temperature plays a secondary, but important role in mitigating the outgassing in both the PFZ and SAZ, where positive SAM leads to colder than normal surface temperatures (Figure 2), and hence large negative ΔT values.

[25] While our analysis of the CO_2 derivative offers a simple way to understand the anomalous outgassing, we find a slight discrepancy between the sum of terms, Σ, and the modeled anomaly in F during positive SAM, ΔF_{mod} (Table 3, last two rows). The approximations used in the pCO_2 calculations (see (A4)–(A9)), or the possible cross correlations among the variables may lead to imprecise results in some of the regions.

[26] Given the importance of *sDIC* variations for causing surface pCO_2^{oc} and air-sea CO_2 flux variations south of the STZ, it is incumbent on us to determine the mechanisms controlling *sDIC* anomalies. To accomplish this, we examine the sources and sinks of the modeled tendency in *sDIC* anomalies,

$$\frac{d(sDIC')}{dt} = J'_{circ} - J'_{bio} - J'_{ex}, \tag{4}$$

where J'_{circ}, J'_{bio}, and J'_{ex} represent the sources and sinks of $sDIC'$ from circulation, biology, and CO_2 flux anomalies. J'_{ex} is the anomaly in modeled air-sea flux of CO_2 divided by the depth of the mixed layer. J'_{bio} represents the sink of $sDIC'$ due to organic and calcium carbonate production (see Appendix B for additional details). The circulation term,

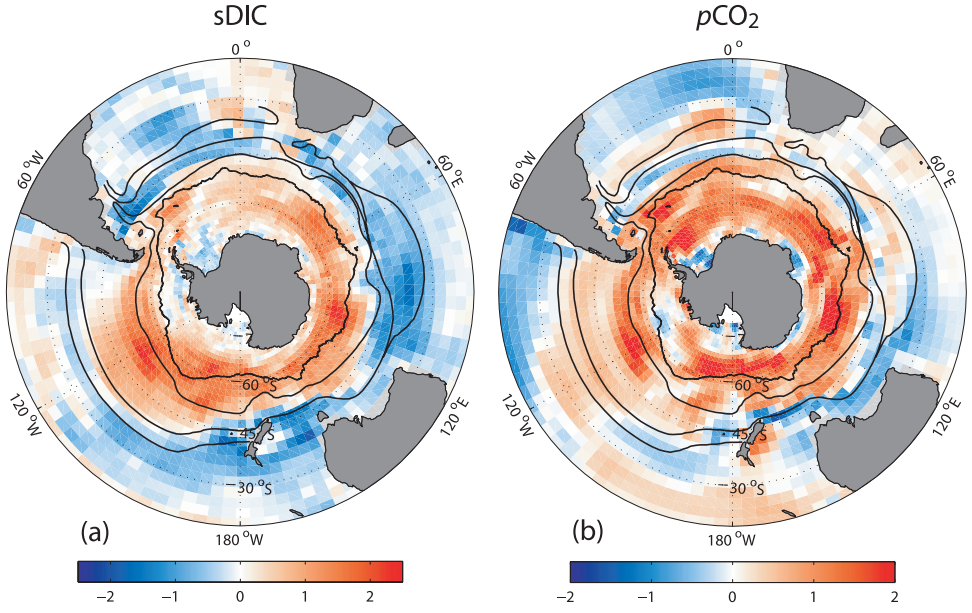

Figure 10. Regression of (a) salinity-normalized surface *DIC* anomalies (mmol m^{-3}) and (b) pCO_2^{oc} anomalies (μatm) from the pre-industrial simulation onto the standardized SAM index.

Table 4. Mean Values and Regression and Correlation Coefficients of the Mean Anomaly Time Series With the SAM Index From the Pre-Industrial Run[a]

Zone	Mean Value	Regression	Correlation
	Air-Sea CO_2 Flux, mol m^{-2} yr^{-1}		
AZ	0.95	0.14	0.56
PFZ	0.78	0.13	0.42
SAZ	−0.68	0.05	0.23
STZ	−0.99	0.02	0.13
	pCO_2^{oc}, μatm		
AZ	294	0.79	0.26
PFZ	280	0.80	0.30
SAZ	268	0.45	0.21
STZ	268	0.09	0.05
	Surface sDIC, mmol m^{-3}		
AZ	2166	0.59	0.36
PFZ	2112	0.81	0.32
SAZ	2061	0.36	0.16
STZ	2002	−0.49	−0.20
	Mixed Layer Depth, m		
AZ	60.76	0.95	0.28
PFZ	96.52	1.97	0.30
SAZ	82.92	0.69	0.09
STZ	95.83	−3.05	−0.27
	Vertical Velocity, cm s^{-1}		
AZ	6.2×10^{-5}	1.0×10^{-5}	0.83
PFZ	2.5×10^{-5}	-0.9×10^{-5}	−0.50
SAZ	-2.6×10^{-5}	-1.2×10^{-5}	−0.70
STZ	-5.3×10^{-5}	-0.7×10^{-6}	−0.45
	Northward Meridional Velocity, cm s^{-1}		
AZ	0.37	0.16	0.85
PFZ	0.95	0.14	0.76
SAZ	1.02	0.02	0.14
STZ	0.91	−0.11	−0.59

[a]Regression coefficients correspond to 1 standard deviation change in the SAM index. Positive air-sea CO_2 flux and vertical velocity correspond to outgassing and upwelling, respectively. Velocities were calculated for the mixed layer.

J'_{circ} is computed by difference. All source and sink terms were calculated for the region south of the SSTF (~42°S), integrated over the annual mean mixed layer.

[27] We report the results of the *sDIC* tendency components in (4) as regressions of the anomaly time series with the SAM index (Table 5). The source of *sDIC* due to circulation dominates the *sDIC* anomaly during positive SAM, with the sinks of natural CO_2 outgassing and biology playing smaller roles. This anomalous circulation driving the *sDIC* source is caused by the stronger overturning in the southernmost regions of the Southern Ocean, which results in a 16% increase in upwelling and a 43% increase in northward meridional velocity in the AZ (Figure 11, Table 4). The upwelling of *sDIC*-rich waters and their subsequent lateral transport creates positive anomalies in surface *sDIC* throughout the AZ, PFZ, and SAZ (Figure 9b). A separate calculation not shown here indicates that the deepening of the mixed layer during positive SAM (Table 4) also has a small effect on the circulation contribution to *sDIC*. Our findings indicate that biological production does not play a particularly important role in controlling surface *sDIC* anomalies during positive SAM (Table 5).

[28] In summary, both wind speed and surface *sDIC* changes during positive SAM influence the flux of natural CO_2 between the atmosphere and the Southern Ocean. We have shown that circulation changes contribute to a large fraction of the *sDIC* anomalies. Similar circulation mechanisms are primarily responsible for the anomalous uptake of anthropogenic CO_2 during positive SAM (Table 5), when anomalous upwelling and meridional transport expose deep, older waters to higher atmospheric CO_2 levels. Positive phases of the SAM are therefore associated with simultaneous natural CO_2 outgassing and anthropogenic CO_2 uptake anomalies in the Southern Ocean. This suggests that the same circulation mechanisms which currently drive enhanced outgassing of natural CO_2 from the Southern Ocean during positive SAM may also play a role in mitigating this response in the future, as the anomalous uptake of anthropogenic CO_2 during positive SAM rises due to increasing atmospheric CO_2 concentrations.

6. Trends in Air-Sea CO_2 Fluxes

[29] Given the responsiveness of air-sea CO_2 fluxes to interannual variations in the SAM, it is worth investigating how the trend in the SAM influences air-sea CO_2 flux. Our results suggest that the observed secular trend in the SAM between 1958 and 2004 toward more positive phases has led to an outgassing trend of natural CO_2 of 0.006 PgC yr^{-2} (Figure 4), with a total increase in the outgassing flux over

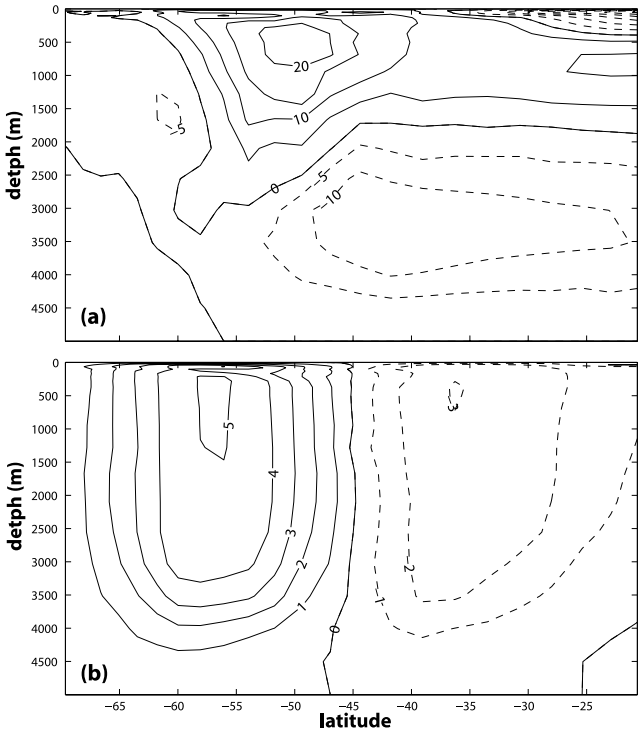

Figure 11. (a) Annual mean meridional overturning stream function (Sv) and (b) regression of meridional overturning anomalies from the pre-industrial simulation onto the standardized SAM index, including the *Gent and McWilliams* [1990] bolus parameterization velocities.

Table 5. Regression Coefficients of the SAM Index With Anomaly Time Series of the Estimated Contributions to the $sDIC'$ Tendency in the Region South of the SSTF, Integrated Over the Mixed Layer, as in Equation (4)[a]

Quantity	Natural	Anthropogenic
$\frac{d(sDIC')}{dt}$	0.25	−0.03
$-J'_{ex}$	−0.09	0.02
$-J'_{bio}$	0.03	0
J'_{circ}	0.31	−0.04

[a]Units are PgC yr^{-1}.

the 47 years of 0.3 PgC yr^{-1}. This trend is masked by the increasing rate of uptake of anthropogenic CO_2, which exhibits a linear trend of −0.011 PgC yr^{-2}, so that the linear contemporary flux trend of −0.005 PgC yr^{-2} is still toward a stronger sink (Figure 4). Nevertheless, the secular trend in the SAM has led to a reduction in the rate of increase of the net uptake of atmospheric CO_2 by the ocean. If this trend persists into the next decade or century, as suggested by some coupled climate models [see, e.g., *Fyfe and Saenko*, 2006], the associated CO_2 outgassing could cause a positive feedback for the global climate system over this time period.

7. Summary

[30] Using a coupled ocean physical-biogeochemical-ecological model, we have demonstrated that the SAM has a significant impact on the flux of CO_2 between the atmosphere and the Southern Ocean under both pre-industrial and historical conditions. During a positive phase of the SAM, we find anomalous outgassing of natural CO_2 nearly everywhere in the Southern Ocean. The outgassing anomalies are concentrated in the AZ, PFZ, and SAZ, where enhanced overturning brings *sDIC*-rich water to the surface and elevates the pCO_2^{oc} (Figure 9). In contrast, there is a simultaneous anomalous uptake of anthropogenic CO_2 during a positive phase of the SAM in the southernmost regions of the Southern Ocean, due to increased upwelling of deep, older waters and their subsequent exposure to higher atmospheric CO_2 levels. The anthropogenic uptake only slightly mitigates the natural outgassing from the Southern Ocean, so that a positive SAM is associated with anomalous outgassing of contemporary CO_2. In a future characterized by higher atmospheric CO_2, however, positive phases of the SAM may be associated with a greater oceanic uptake of anthropogenic CO_2.

[31] Our findings are supported by a recent study by A. H. Butler et al. (Observed relationships between the Southern Annular Mode and atmospheric carbon dioxide, submitted to *Global Biogeochemical Cycles*, 2007) who investigate the role of the SAM in atmospheric CO_2 concentration variability. They find that positive phases of the SAM are associated with both an elevated rate of increase of atmospheric CO_2 at Palmer Station on the Antarctic Peninsula, and an increase in the flux of CO_2 into the atmosphere from the Southern Ocean. These results inspire confidence in our findings for anomalous outgassing of contemporary CO_2 during positive SAM.

[32] Mounting evidence for a positive trend in the SAM index over the past few decades suggests that the mechanisms we describe here will continue to play an important role in the global carbon cycle over the next century [see *Russell et al.*, 2006]. The impact of future secular trends in the SAM on Southern Ocean air-sea CO_2 flux will compete with climate driven effects, such as increased stratification [e.g., *Fung et al.*, 2005]. The mechanisms we describe here may have also been responsible for past climatic variability. *Toggweiler et al.* [2006] hypothesize that a feedback exists between the position of the midlatitude westerlies and the atmospheric CO_2 concentrations on paleoclimatic timescales, and that these mechanisms are key for explaining the large CO_2 variations between glacial and interglacial times. Although our simulations cannot test this hypothesis, they do highlight the important role of the Southern Ocean for the global carbon cycle.

Appendix A: The pCO_2 Calculations

[33] Anomalous pCO_2 during positive SAM (ΔpCO_2^{oc}) is decomposed into the contributions from *DIC*, *Alk*, *T*, and *S* according to (2). To separate the contribution from freshwater fluxes on *DIC* and *Alk*, we use the following two equations for the first and second terms of (2),

$$\frac{\partial pCO_2^{oc}}{\partial DIC}\Delta DIC = \frac{\partial pCO_2^{oc}}{\partial (S/S_0\ \mathrm{sDIC})}\Delta(S/S_0\ \mathrm{sDIC}) = \frac{sDIC}{S_0}\frac{\partial pCO_2^{oc}}{\partial DIC}\Delta S + \frac{S}{S_0}\frac{\partial pCO_2^{oc}}{\partial DIC}\Delta sDIC \quad \text{(A1)}$$

$$\frac{\partial pCO_2^{oc}}{\partial Alk}\Delta Alk = \frac{\partial pCO_2^{oc}}{\partial (S/S_0\ \mathrm{sAlk})}\Delta(S/S_0\ \mathrm{sAlk}) = \frac{sAlk}{S_0}\frac{\partial pCO_2^{oc}}{\partial Alk}\Delta S + \frac{S}{S_0}\frac{\partial pCO_2^{oc}}{\partial Alk}\Delta sAlk. \quad \text{(A2)}$$

We extract the first terms from (A1) and (A2), as they represent the contribution from freshwater forcing (*fw*) on pCO_2^{oc} and account for variability in lateral/vertical circulation working on gradients in salinity,

$$\frac{\partial pCO_2^{oc}}{\partial fw}\Delta fw = \frac{sDIC}{S_0}\frac{\partial pCO_2^{oc}}{\partial DIC}\Delta S + \frac{sAlk}{S_0}\frac{\partial pCO_2^{oc}}{\partial Alk}\Delta S. \quad \text{(A3)}$$

The flux contributions from each region and each process are shown in Table 3.

[34] We use the following set of equations to approximate the regional mean values of the pCO_2^{oc} partial derivatives, using the regional mean values of *DIC*, *Alk*, pCO_2^{oc}, and *S* [*Sarmiento and Gruber*, 2006],

$$\frac{\partial pCO_2^{oc}}{\partial DIC} = \frac{pCO_2^{oc}}{DIC}\cdot\gamma_{DIC} \quad \text{(A4)}$$

$$\frac{\partial pCO_2^{oc}}{\partial Alk} = \frac{pCO_2^{oc}}{Alk}\cdot\gamma_{Alk} \quad \text{(A5)}$$

$$\frac{\partial pCO_2^{oc}}{\partial T} \approx pCO_2^{oc} \cdot 0.0423^\circ C^{-1} \quad \text{(A6)}$$

$$\frac{\partial pCO_2^{oc}}{\partial S} \approx \frac{pCO_2^{oc}}{S}, \quad \text{(A7)}$$

where the buffer factors can be approximated with [*Sarmiento and Gruber*, 2006]

$$\gamma_{DIC} \approx \frac{3 \cdot Alk \cdot DIC - 2 \cdot DIC^2}{(2 \cdot DIC - Alk)(\mathrm{Alk} - \mathrm{DIC})} \quad \text{(A8)}$$

$$\gamma_{Alk} \approx -\frac{Alk^2}{(2 \cdot DIC - Alk)(\mathrm{Alk} - \mathrm{DIC})}. \quad \text{(A9)}$$

Appendix B: Biological Fluxes

[35] The biological sink to the *sDIC* anomaly tendency, J'_{bio}, can be defined as

$$J'_{bio} = \frac{\Phi'_{bio}}{h}, \quad \text{(B1)}$$

where h is the depth of the mixed layer and Φ'_{bio} represents the anomalies in the biological flux, defined as the sum of anomalies in the flux of organic carbon and calcium carbonate across the depth of the mixed layer,

$$\Phi'_{bio} = \Phi'_{org} + \Phi'_{CaCO_3}. \quad \text{(B2)}$$

Φ'_{org} is approximated by the anomalous flux of particulate organic carbon, as the anomalous flux of dissolved organic carbon is very small. Substitution of (B2) into (B1) yields

$$J'_{bio} = \frac{1}{h}\left(\Phi'_{org} + \Phi'_{CaCO_3}\right). \quad \text{(B3)}$$

[36] **Acknowledgments.** This work was supported by NASA headquarters under the Earth System Science Fellowship Grant NNG05GP78H to N. S. L. and grants NAG5-12528 and NNG04GH53G to N. G. Both S. C. D. and I. D. L. were supported by NSF/ONR NOPP (N000140210370) and NASA (NNG05GG30G). We thank D. Thompson, A. Butler, and S. Denning for many stimulating discussions. Constructive reviews from J. R. Toggweiler and one anonymous reviewer are gratefully acknowledged.

References

Belkin, I. M., and A. L. Gordon (1996), Southern Ocean fronts from the Greenwich meridian to Tasmania, *J. Geophys. Res.*, *101*(C2), 3675–3696.

Bousquet, P., P. Peylin, P. Ciais, C. LeQuéré, P. Friedlingstein, and P. P. Tans (2000), Regional changes in carbon dioxide fluxes of land and oceans since 1980, *Science*, *290*, 1342–1346.

Bretherton, C. S., M. Widmann, V. P. Dymnikov, J. M. Wallace, and I. Bladé (1999), The effective number of spatial degrees of freedom of a time-varying field, *J. Clim.*, *12*(7), 1990–2009.

Brix, H., N. Gruber, and C. D. Keeling (2004), Interannual variability of the upper ocean carbon cycle at station ALOHA near Hawaii, *Global Biogeochem. Cycles*, *18*, GB4019, doi:10.1029/2004GB002245.

Carril, A. F., C. G. Menendez, and A. Navarra (2005), Climate response associated with the Southern Annnular Mode in the surroundings of Antarctic Peninsula: A multimodel ensemble analysis, *Geophys. Res. Lett.*, *32*, L16713, doi:10.1029/2005GL023581.

Doney, S. C., K. Lindsay, I. Fung, and J. John (2006), Natural variability in a stable 1000 year coupled climate-carbon cycle simulation, *J. Clim.*, *19*(13), 3033–3054.

Doney, S. C., S. Yeager, G. Danabasoglu, W. G. Large, and J. C. McWilliams (2007), Mechanisms governing interannual variability of upper ocean temperature in a global hindcast simulation, *J. Phys. Oceanogr.*, in press.

Dore, J. E., R. Lukas, D. Sadler, and D. M. Karl (2003), Climate-driven changes to the atmospheric CO_2 sink in the subtropical North Pacific Ocean, *Nature*, *424*, 754–757.

Fung, I., S. C. Doney, K. Lindsay, and J. John (2005), Evolution of carbon sinks in a changing climate, *Proc. Natl. Acad. Sci. U. S. A.*, *102*, 11,201–11,206, doi:10.1073/pnas.0504949102.

Fyfe, J. C., and O. A. Saenko (2006), Simulated changes in the extratropical Southern Hemisphere winds and currents, *Geophys. Res. Lett.*, *33*, L06701, doi:10.1029/2005GL025332.

Gent, P. R., and J. C. McWilliams (1990), Isopycnal mixing in ocean circulation models, *J. Phys. Oceanogr.*, *20*(1), 150–155.

Gruber, N., C. D. Keeling, and N. R. Bates (2002), Interannual variability in the North Atlantic Ocean carbon sink, *Science*, *298*, 2374–2378.

Gruber, N., P. Friedlingstein, C. B. Field, R. Valentini, M. Heimann, J. E. Richey, P. Romero-Lankao, D. Schulze, and C.-T. A. Chen (2004), The vulnerability of the carbon cycle in the 21st century: An assessment of carbon-climate-human interactions, in *The Global Carbon Cycle: Integrating Humans, Climate, and the Natural World*, edited by C. B. Field and M. R. Raupach, pp. 45–76, Island, Washington, D. C.

Hall, A., and M. Visbeck (2002), Synchronous variability in the Southern Hemisphere atmosphere, sea ice, and ocean resulting from the annular mode, *J. Clim.*, *15*(21), 3043–3057.

Hartmann, D. L., and F. Lo (1998), Wave-driven zonal flow vacillation in the Southern Hemisphere, *J. Atmos. Sci.*, *55*(8), 1303–1315.

Hughes, C. W., P. l. Woodworth, M. P. Meredith, V. Stepanov, T. Whitworth, and A. R. Pyne (2003), Coherence of Antarctic sea levels, Southern Hemisphere Annular Mode, and flow through Drake Passage, *Geophys. Res. Lett.*, *30*(9), 1464, doi:10.1029/2003GL017240.

Joos, F., G.-K. Plattner, T. F. Stocker, O. Marchal, and A. Schmittner (1999), Global warming and marine carbon cycle feedbacks on future atmospheric CO_2, *Science*, *284*, 464–467.

Kalnay, E., et al. (1996), The NCEP/NCAR 40-Year Reanalysis Project, *Bull. Am. Meteorol. Soc.*, *77*(3), 437–470.

Keeling, C. D., H. Brix, and N. Gruber (2004), Seasonal and long-term dynamics of the upper ocean carbon cycle at Station ALOHA near Hawaii, *Global Biogeochem. Cycles*, *18*, GB4006, doi:10.1029/2004GB002227.

Large, W., and S. G. Yeager (2004), Diurnal to decadal global forcing for ocean and sea-ice models: The datasets and flux climatologies, *NCAR Tech. Note, NCAR/TN-460 STR*, 105 pp.

Lefévre, N., A. J. Watson, A. Olsen, A. F. Ríos, F. F. Pérez, and T. Johannessen (2004), A decrease in the sink for atmospheric CO_2 in the North Atlantic, *Geophys. Res. Lett.*, *31*, L07306, doi:10.1029/2003GL018957.

Lenton, A., and R. Matear (2007), Role of the Southern Annular Mode (SAM) in Southern Ocean CO_2 uptake, *Global Biogeochem. Cycles*, *21*, GB2016, doi:10.1029/2006GB002714.

LeQuéré, C., J. C. Orr, P. Monfray, and O. Aumont (2000), Interannual variability of the oceanic sink of CO_2 from 1979 through 1997, *Global Biogeochem. Cycles*, *14*(4), 1247–1265.

Limpasuvan, V., and D. L. Hartmann (1999), Eddies and the annular modes of climate variability, *Geophys. Res. Lett.*, *26*(20), 3133–3136.

Liu, J., J. A. Curry, and D. G. Martinson (2004), Interpretation of recent Antarctic sea ice variability, *Geophys. Res. Lett.*, *31*, L02205, doi:10.1029/2003GL018732.

Lovenduski, N. S., and N. Gruber (2005), Impact of the Southern Annular Mode on Southern Ocean circulation and biology, *Geophys. Res. Lett.*, *32*, L11603, doi:10.1029/2005GL022727.

Mahowald, N., C. Luo, J. del Corral, and C. S. Zender (2003), Interannual variability in atmospheric mineral aerosols from a 22-year model simulation and observational data, *J. Geophys. Res.*, *108*(D12), 4352, doi:10.1029/2002JD002821.

Matear, R. J., and A. C. Hirst (1999), Climate change feedback on the future oceanic CO_2 uptake, *Tellus, Ser. B*, *51*, 722–733.

McCartney, M. S. (1982), The subtropical recirculation of Mode Waters, *J. Mar. Res.*, *40*, suppl., 427–464.

McKinley, G. A., M. J. Follows, and J. Marshall (2004), Mechanisms of air-sea CO_2 flux variability in the equatorial Pacific and the North Atlantic, *Global Biogeochem. Cycles*, *18*(2), GB2011, doi:10.1029/2003GB002179.

Mikaloff-Fletcher, S. E., et al. (2006), Inverse estimates of anthropogenic CO_2 uptake, transport, and storage by the ocean, *Global Biogeochem. Cycles*, *20*, GB2002, doi:10.1029/2005GB002530.

Mikaloff-Fletcher, S. E., et al. (2007), Inverse estimates of the oceanic sources and sinks of natural CO_2 and the implied oceanic carbon transport, *Global Biogeochem. Cycles*, *21*, GB1010, doi:10.1029/2006GB002751.

Moore, J. K., M. R. Abbott, and J. G. Richman (1999), Location and dynamics of the Antarctic Polar Front from satellite sea surface temperature data, *J. Geophys. Res.*, *104*(C2), 3059–3073.

Moore, J. K., S. C. Doney, and K. Lindsay (2004), Upper ocean ecosystem dynamics and iron cycling in a global 3-D model, *Global Biogeochem. Cycles*, *18*, GB4028, doi:10.1029/2004GB002220.

Moore, J. K., S. C. Doney, K. Lindsay, N. Mahowald, and A. F. Michaels (2006), Nitrogen fixation amplifies the ocean biogeochemical response to decadal timescale variations in mineral dust deposition, *Tellus, Ser. B*, *58*, 560–572.

Murnane, R. J., J. L. Sarmiento, and C. LeQuéré (1999), Spatial distribution of air-sea CO_2 fluxes and the interhemispheric transport of carbon by the oceans, *Global Biogeochem. Cycles*, *13*(2), 287–305.

Oke, P. R., and M. H. England (2004), Oceanic response to changes in the latitude of the Southern Hemisphere subpolar westerly winds, *J. Clim.*, *17*(5), 1040–1054.

Peylin, P., P. Bousquet, C. LeQuéré, S. Sitch, P. Friedlingstein, G. McKinley, N. Gruber, P. Rayner, and P. Ciais (2005), Multiple constraints on regional CO_2 flux variations over land and oceans, *Global Biogeochem. Cycles*, *19*, GB1011, doi:10.1029/2003GB002214.

Plattner, G.-K., F. Joos, T. F. Stocker, and O. Marchal (2001), Feedback mechanisms and sensitivities of ocean carbon uptake under global warming, *Tellus, Ser. B*, *53*, 564–592.

Rintoul, S. R., C. W. Hughes, and D. Olbers (2001), The Antarctic Circumpolar Current System, in *Ocean Circulation and Climate*, edited by G. Siedler, J. Church, and J. Gould, pp. 271–302, Academic, San Diego, Calif.

Russell, J. L., K. W. Dixon, A. Gnanadesikan, R. J. Stouffer, and J. R. Toggweiler (2006), The Southern Hemisphere westerlies in a warming world: Propping open the door to the deep ocean, *J. Clim.*, *19*(24), 6382–6390.

Sabine, C. L., et al. (2004), The oceanic sink for anthropogenic CO_2, *Science*, *305*, 367–371.

Sarmiento, J. L., and N. Gruber (2006), *Ocean Biogeochemical Dynamics*, Princeton Univ. Press, Princeton, N. J.

Sarmiento, J. L., and J. R. Toggweiler (1984), A new model for the role of the oceans in determining atmospheric pCO_2, *Nature*, *308*, 621–624.

Sarmiento, J. L., T. M. C. Hughes, R. J. Stouffer, and S. Manabe (1998), Simulated response of the ocean carbon cycle to anthropogenic climate warming, *Nature*, *393*, 245–249.

Siegenthaler, U., and T. Wenk (1984), Rapid atmospheric CO_2 variations and ocean circulation, *Nature*, *308*, 624–626.

Thompson, D. W. J., and S. Solomon (2002), Interpretation of recent Southern Hemisphere climate change, *Science*, *296*, 895–899.

Thompson, D. W. J., and J. M. Wallace (2000), Annular modes in the extratropical circulation. Part I: Month-to-month variability, *J. Clim.*, *13*(5), 1000–1016.

Thompson, D. W. J., J. M. Wallace, and G. C. Hegerl (2000), Annular modes in the extratropical circulation. Part II: Trends, *J. Clim.*, *13*(5), 1018–1036.

Toggweiler, J. R., and B. Samuels (1993), New radiocarbon constraints on the upwelling of abyssal water to the ocean's surface, in *The Global Carbon Cycle*, edited by M. Heimann, pp. 333–366, Springer, New York.

Toggweiler, J. R., J. L. Russell, and S. R. Carson (2006), Midlatitude westerlies, atmospheric CO_2, and climate change during the ice ages, *Paleoceanography*, *21*, PA2005, doi:10.1029/2005PA001154.

Wanninkhof, R. (1992), Relationship between wind speed and gas exchange over the ocean, *J. Geophys. Res.*, *97*(C5), 7373–7382.

Watson, A., and J. Orr (2003), Carbon dioxide fluxes in the global ocean, in *Ocean biogeochemistry: The Role of the Ocean Carbon Cycle in Global Change*, edited by M. J. R. Fasham, pp. 123–143, Springer, Berlin.

Watterson, I. G. (2000), Southern midlatitude zonal wind vacillation and its interaction with the ocean in GCM simulations, *J. Clim.*, *13*(3), 562–578.

Wetzel, P., A. Winguth, and E. Maier-Reimer (2005), Sea-to-air CO_2 flux from 1948 to 2003: A model study, *Global Biogeochem. Cycles*, *19*, GB2005, doi:10.1029/2004GB002339.

Yeager, S. G., C. A. Shields, W. G. Large, and J. J. Hack (2006), The low-resolution CCSM3, *J. Clim.*, *19*(11), 2545–2566.

S. C. Doney and I. D. Lima, Department of Marine Chemistry and Geochemistry, Woods Hole Oceanographic Institution, Woods Hole, MA 02543-1543, USA. (sdoney@whoi.edu; ilima@whoi.edu)

N. Gruber, Environmental Physics, Institute of Biogeochemistry and Pollutant Dynamics, CHN E21.1, Universitaetstr. 16, ETH Zurich, CH-8092 Zurich, Switzerland. (nicolas.gruber@env.ethz.ch)

N. S. Lovenduski, Department of Atmospheric and Oceanic Sciences, University of California, Los Angeles, 405 Hilgard Ave, Box 951565, Los Angeles, CA 90095-1565, USA. (nikki@atmos.ucla.edu)